Micro-macro experimental investigation into the thermomechanical volumetric response of non-active clay

Citation for the original published paper (version of record):
Casarella, A., Tarantino, A., Di Donna, A. (2026). Micro-macro experimental investigation into the thermomechanical volumetric response of
non-active clay. Geomechanics for Energy and the Environment, 46.
http://dx.doi.org/10.1016/j.gete.2026.100831

Geomechanics for Energy and the Environment 46 (2026) 100831

Contents lists available at ScienceDirect

Geomechanics for Energy and the Environment

journal homepage: www.elsevier.com/locate/gete

Micro-macro experimental investigation into the thermomechanical volumetric response of non-active clay

Angela Casarella [a,b,*], Alessandro Tarantino [c], Alice di Donna [a]

[a] Univ. Grenoble Alpes, CNRS, Grenoble INP, 3SR, Grenoble 38000, France
[b] Chalmers University of Technology, Department of Architecture and Civil Engineering, Gothenburg 43218, Sweden
[c] University of Strathclyde, Department of Civil and Environmental Engineering, Glasgow, Scotland G1 1XJ, UK

ARTICLE INFO

Editors-in-Chief: Professor Lyesse Laloui and Professor Tomasz Hueckel

Keywords:
Clay
Thermomechanical behaviour
MIP
PSD
Particle-scale mechanism

ABSTRACT

The thermomechanical behaviour of clayey soils is critical for various geotechnical and geoenvironmental applications, yet the underlying particle-scale mechanisms remain debated. This study presents a multi-scale investigation into the microstructural origins of the distinct volumetric responses observed in normally consolidated (NC) and overconsolidated (OC) clays subjected to thermal loading. Temperature-controlled isotropic compression tests were coupled with Mercury Intrusion Porosimetry (MIP) on reconstituted samples of Speswhite Kaolin clay.

The macroscopic results confirm that NC non-active clay exhibits irreversible contraction upon heating, while highly OC non-active clay undergoes reversible expansion. MIP analyses reveal that thermal contraction in NC kaolin is linked to a reduction in macropore volume, driven by irreversible slippage at edge-to-face particle contacts due to a temperature-induced weakening of electrochemical attractions. In contrast, the thermal expansion of OC clay is associated with an elastic increase in the separation distance between face-to-face particle configurations.

These findings provide direct experimental support for recent particle-scale modelling based on 3D DLVO interactions and demonstrate that thermal loading under constant stress activates the same microscale processes that drive mechanically induced volumetric deformation. The high level of experimental control makes the resulting dataset particularly suited for validation of particle-scale numerical models and for informing constitutive formulations that explicitly link thermomechanical behaviour to interparticle forces and contact mechanics.

1. Introduction

The impact of temperature on mechanical behaviour of geomaterials is of increasing concern in geoenvironmental engineering. Over the past decades, considerable attention has been devoted to studying the response of fine-grained soils to the combined effects of stress and temperature, particularly in the context of nuclear waste geological disposal[1-3]. This research has predominantly focused on high-swelling clay subjected to elevated temperatures and pressures resulting from the confinement of the engineered barrier system. On the other hand, the investigation into the effects of temperature changes on mechanical behaviour of non-active or moderately active clay has been relatively limited despite their relevance to various applications such as shallow geothermal plants[4], energy geostructures[5], and heating in rapid shear deformation[6]. Non-active clays are clays with low mineralogical activity, meaning they show limited particle swelling, low cation exchange capacity, and small amounts of adsorbed water, in contrast to highly active clays such as smectites. This makes their thermomechanical behaviour distinct from that of highly active clays and motivates dedicated investigation.

The observed mechanical response of (saturated) clay to temperature variation is not always intuitive. Clay exhibits irreversible contraction in normally consolidated (NC) states and reversible expansion in highly overconsolidated (OC) states upon heating and subsequent cooling [7,8,3,9,10]. Modelling such a complex, non-linear and irreversible behaviour requires advanced constitutive models. During the last thirty years, several 'phenomenological' elastoplastic models have been developed to consider the effects of temperature variations on the behaviour of clayey

* Corresponding author at: Univ. Grenoble Alpes, CNRS, Grenoble INP, 3SR, Grenoble 38000, France.
E-mail address: a.casarella@imperial.ac.uk (A. Casarella).

https://doi.org/10.1016/j.gete.2026.100831
Received 17 June 2025; Received in revised form 8 April 2026; Accepted 11 April 2026
Available online 13 April 2026

soils[11–14]. While these models provide valuable macroscopic predictions, a mechanistic understanding of thermomechanical behaviour at the particle scale is still lacking.

Early attempts to describe clay particle-scale mechanisms under thermal loading focused on the analysis of (i) the thermoelastic strain of the clay skeleton and (ii) the combined effective thermal expansion of the adsorbed water (Campanella and Mitchell, 1968). All the soil constituents (i.e. solid minerals, adsorbed, and free water) dilate when temperature increases. Under drained conditions, the effects of free water thermal expansion dissipate with time, depending on the medium's permeability. On the contrary, the thermal volume change of adsorbed water and minerals produces a macroscopic thermal strain related to temperature variation[15].

The expected volumetric thermal expansion computed according to the thermal dilation of the clay constituents (solid mineral and water) reasonably follows the thermal dilation observed in the literature in highly OC conditions[16]. However, uncertainties remain concerning basic mechanisms involved in the thermal volumetric 'collapse' observed in NC clay.

Baldi et al.[15] attributed the NC thermal contraction to the physiochemical interactions between clay and water, which, in turn, is associated with the variation of the thickness of the double layer due to temperature changes. An increase in temperature would result in the removal of bound water molecules and, hence, an irreversible decrease in the double layer thickness, as also hypothesised by Olson and Mesri[17] and Morin and Silva[18] and numerically proven more recently using fully atomistic molecular dynamics by Brochard et al.[19]. More recent constitutive modelling efforts have incorporated thermo-poromechanical couplings to capture the role of bound water dehydration in the thermoplastic strain recorded in NC clays upon heating[2]. However, for low-activity, large-particle clays such as kaolinite, the proportion of adsorbed (bound) water is typically limited to only a few percent of the total water content[20]. Consequently, temperature-induced variations in bound water are expected to generate volumetric strains that are small compared to the plastic strains observed experimentally for example in Cekerevac and Laloui[7], suggesting that physicochemical effects alone are insufficient to explain the magnitude of thermally induced contraction in such materials.

Several studies have also hinted at the mechanisms of particle rearrangement at the microscopic (and nanoscopic) scale to explain the related thermally-induced contraction observed at the macroscopic scale. Towhata et al.[1] associated the decrease in the shearing strength of clay upon heating with the modification of the contact force network due to the different thermal expansion of the clay minerals involved. This decrease in inter-particle strength increases the probability of particle slippage, which is maximised when the mobilised force producing such slippage is higher.

While quantitative microstructural investigations tracking pore-scale and fabric evolution are well established in studies of purely mechanical loading[21,22], their extension to thermally induced deformation remains limited. Building on the conceptual framework proposed by Towhata et al.[1], the first microscopic observation to detect a possible particle re-orientation due to temperature changes can be found in Houhou et al.[23]. The experimental campaign, conducted via MIP and XCT tests on remoulded samples of NC kaolinite and illite, revealed significant changes in the pore size distribution (PSD) of the illite specimens after thermal loading. In kaolinite samples, no appreciable changes in PSD were recorded. Houhou et al.[23] concluded by ascribing the thermal volumetric collapse in NC clay to changes in the contact particles network induced by the combination of thermal and mechanical load and hypothesised that modifications of the diffuse double layer due to temperature changes would not be the main reason behind the observed thermally-induced volumetric strain.

Under the same line of reasoning, Di Donna et al.[24] investigated the electrochemical and contact interactions between clay particles under thermomechanical loading with a combined numerical and analytical approach. It was concluded that the electrochemical interactions (governing the face-to-face particle configuration) can only explain the elastic volumetric response of OC clays subjected to heating. The thermo-plastic behaviour typical of NC clays was attributed to changes in the contact force in the edge-to-face particle configurations. These findings represent a significant step toward identifying the governing microscale driving volumetric collapse upon heating in NC clays mechanisms but remain largely inferential, as direct experimental evidence quantitatively linking particle-scale rearrangement to macroscopic thermal strains remains scarce.

Building on this context, an important gap becomes evident. Current constitutive models implicitly assume that the microscale mechanisms activated by thermal loading are analogous to those mobilised during mechanical compression, yet this assumption has never been experimentally verified at the particle scale. Consequently, it remains unclear whether thermally induced volumetric changes in NC clays arise from a fundamentally different class of microscale processes, or whether heating simply triggers mechanically equivalent volumetric deformation pathways under constant stress. This paper addresses this gap through a multi-scale investigation of the thermomechanical volumetric response of a non-active clay. By directly comparing thermally induced and mechanically induced microstructural changes, the goal of this study is to provide new experimental evidence about whether that thermal volumetric deformation at the particle scale exhibits or not strong similarities to mechanical volumetric deformation.

Temperature-controlled isotropic compression tests were coupled with Mercury Intrusion Porosimetry (MIP) tests to explore microstructural changes in reconstituted normally consolidated and overconsolidated samples of Speswhite Kaolin clay specimens subjected to mechanical and thermal loading. Additional Scanning Electron Microscope (SEM) observations were aimed to support qualitatively the mechanistic interpretation rather than providing a quantitative validation.

The macroscopic tests have been performed in a newly developed temperature-controlled isotropic compression cell equipped with an accurate pore-water pressure monitoring system, ensuring strictly drained conditions throughout heating and cooling phases. Combined with the use of a relatively uniform model clay with a relatively uniform particle size distribution and a controlled sample preparation procedure and pore fluid environment, these experimental conditions were aimed to ensure a highly reproducible testing framework and facilitate the interpretation of the experimental results.

2. Material and sample preparation

2.1. Material

Commercially available Speswhite Kaolin clay (IMERYS, France) with plastic limit $w_P = 0.32$ and liquid limit $w_L = 0.64$ was chosen for the tests presented in this paper. The grain size distribution reveals 80% clay fraction (<0.002 mm), 20% silt fraction (<0.05 mm), and a median particle diameter of $D_{50} = 1.3\mu m$.

To prepare the samples, Speswhite Kaolin clay powder was mixed with de-ionised de-aired water with an electrical conductivity of 20μS/cm at 25°C and pH $= 4.0 \pm 0.2$ to create a suspension of 100 g of kaolinite per litre of water. The suspension was left to settle for 72 h before the supernatant liquid conductivity was first measured. The clay was considered 'monoionic with no excess salts' (concentration of salt $<10^{-5}$mol/L) when the supernatant liquid conductivity was < 100μS/cm[25]. If this was not the case, the supernatant liquid was siphoned, and the excess salt was removed through several further washings with de-ionised de-aired water. When the desired conductivity was reached, the clay was oven-dried and ground into powder using a pestle and mortar. This procedure allowed controlling the ionic strength of the pore fluid, which affects significantly the mechanical properties of the clay.

Specimens for all tests were prepared with acidic de-ionised de-aired

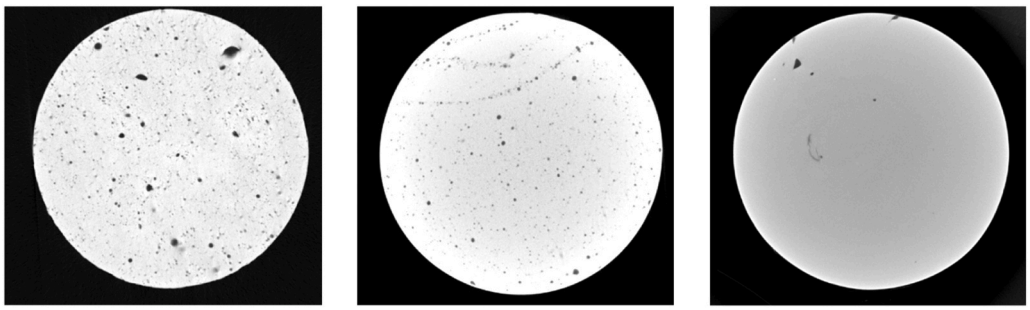

SLURRY_1.5LL
Demineralized water (w=1.5 LL) was added to the powder and manually mixed

SLURRY_MIX_2LL
Demineralized water (w=2.0 LL) was added to the powder, mechanically mixed, vibrated

SLURRY_SEDIMENT_5LL
Clay powder was sieved (0.5 mm sieve) and added to a column of water and let sediment

(a) (b) (c)

Fig. 1. X-ray computed tomography horizontal cross-sections of 1D-compressed samples (σ'_v = 200 kPa, Φ_{ini}=38 ± 1 mm) prepared with three different slurry preparation protocols and to be tested in the isotropic compression cell.

Table 1
Physical properties of the samples tested in the experimental campaign at the initial state.

Diameter	Φ_{ini}	38 ± 1 mm
Height	h_{ini}	76 ± 5 mm
Unit weight of the grains	γ_s	26.0 kN/m^3
Unit dry weight of the sample	γ	12.0 ± 2.0 kN/m^3
Water content	w_{conso}	46 ± 2%

water with a target pH of the clay-water mixture of 4.5. The pH was adjusted using HNO_3 2%. The acidic pore fluid was aimed at generating a card-house structure before heating[26].

2.2. Sample preparation

Three different sample preparation procedures were investigated to ensure adequate sample homogeneity and repeatability:

- **Slurry_1.5LL**: acidic de-ionised de-aired water was manually mixed with clay powder oven-dried at 50ºC to achieve a water content $w_{slurry} = 1.5w_L = 96\%$[27]. The slurry was poured into a consolidometer of 170 mm in diameter and consolidated to 200 kPa vertical stress.
- **Slurry_MIX_2LL**: acidic de-ionised de-aired water was mechanically mixed (electric mixer at 700 RPM) with clay powder oven-dried at 50ºC to a water content $w_{slurry} = 2w_L = 128\%$ directly in the consolidometer. Before consolidation, the consolidometer was placed on a shaker table, and the slurry was vibrated under vacuum at 125 RPM for 20 min. The slurry was then consolidated to 200 kPa vertical stress.
- **Slurry_SEDIMENT_5LL**: the slurry was obtained by sedimentation of pluviated (passing through a 0.5 mm sieve) oven-dried kaolinite powder into the 170 mm diameter and 120 cm high consolidometer filled with acidic de-ionised de-aired water (clay concentration of the suspension equal to 320 g/L which corresponds to $w_{suspension} = 5w_L = 320\%$). Kaolinite particles were left to settle until a clear supernatant liquid was visible on the sediment. Once the sediment height reached equilibrium, the supernatant water was removed from the cylinder by siphoning. The effective stress was initially increased up to 20 kPa by imposing suction with a negative water column. The sediment was finally consolidated to 200 kPa vertical stress.

Clay specimens 38 mm diameter and 76 mm high were trimmed from the 170 mm diameter clay cakes. The homogeneity of the samples prepared according to the three different procedures was analysed by X-ray Computed Tomography (XCT) at Laboratoire 3SR in Grenoble, France.

Fig. 1 shows the horizontal cross-sections of the three 38 mm diameter samples. The sample obtained with the first method (Slurry_MIX_1.5LL, Fig. 1a presents many air cavities up to size of 3 mm) is therefore highly inhomogeneous. Although this slurry preparation technique is often employed in manufacturing remoulded clay samples for triaxial and isotropic compression testing, this method was abandoned.

Increasing the initial moisture content of the slurry reduced the size of the air cavities in the specimen (Slurry_MIX_2LL in Fig. 1b, air cavity size up to 1 mm). Nonetheless, the Slurry_MIX_2LL technique still could not ensure homogeneity.

The sample prepared by sedimentation (Slurry_SEDIMENT_5LL, Fig. 1c) showed indeed good uniformity of the clay matrix (similar findings are reported by[28]). No micro-cavities could be detected in the scan. If any cavities were present, their size must have been smaller than the pixel size (=46.1 μm).

All samples tested in this experimental campaign were prepared according to Slurry_SEDIMENT_5LL preparation protocol. A summary of the properties of the specimens after consolidation and prior to isotropic testing is given in Table 1.

3. Test equipment and procedures

3.1. Isotropic cell

The newly developed isotropic cell was designed to test saturated clay specimens of 38 mm diameter and 76 mm height subjected to isotropic total stress and temperature to be increased or decreased independently at controlled rate (Fig. 2).

The main body consists of a 30-mm thick stainless-steel cylinder surrounded by four flexible silicon rubber electrical heaters and externally enclosed by an insulation system made of glass wool to prevent heat dissipation. The cap, the bottom of the cell, the sample pedestal and all lines are made of stainless steel. Stainless steel was also adopted for the drainage lines to ensure thermal and mechanical compatibility with the cell components, thereby minimising differential thermal expansion and compliant deformation during temperature variations.

Water has been chosen as the confining fluid because of the relatively limited confining pressure to be applied (up to 2 MPa). The maximum testing temperature has been limited to 90ºC. Neoprene membranes were employed, better suited to long-term use in high-temperature (up to 120ºC) applications than standard latex membranes.

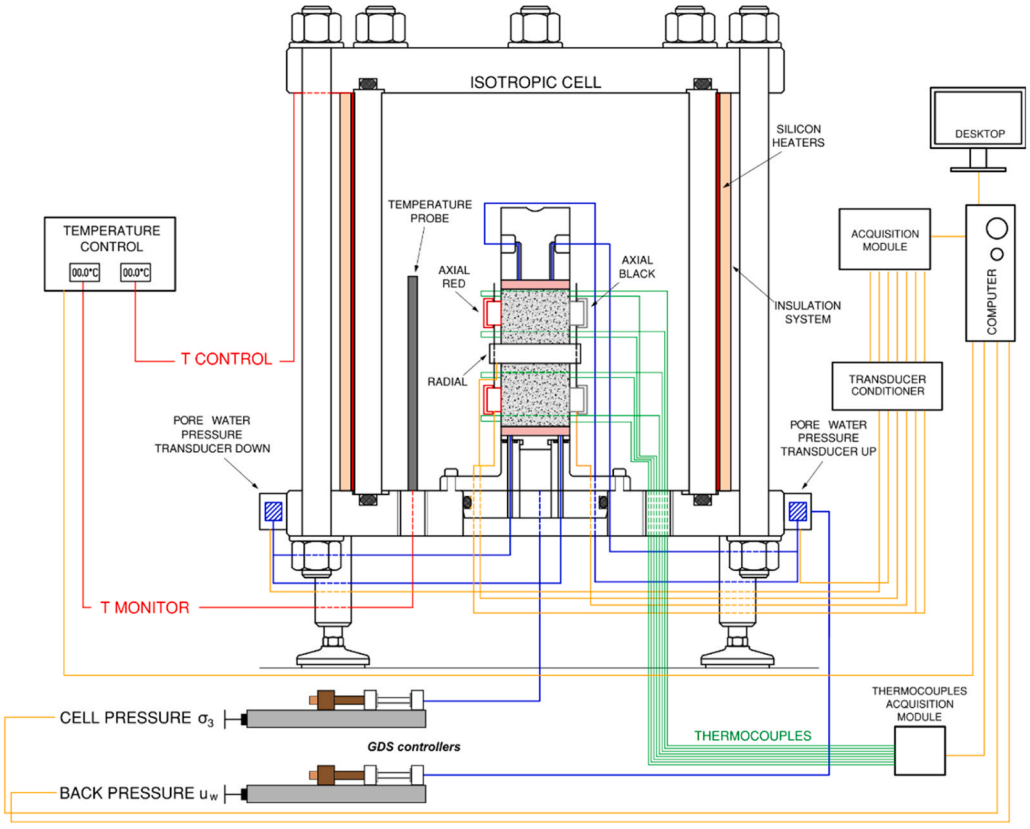

Fig. 2. Temperature-controlled isotropic compression cell setup.

Table 2
Summary of testing conditions for all the macroscopically tested samples of Speswhite Kaolin clay.

Sample		Stress state				Temperature [°C]	
Initial void ratio, e_{ini}	Test ID	Stress history	OCR	Confinement stress, p'_c	Preconsolidation stress, p'_p	Thermal cycle, TC	TC range
1.27 ± 0.05	K1-SW-I250	NC	1	250 kPa	250 kPa	NO	25
1.29 ± 0.05	K1-SW-IT250	NC	1	250 kPa	250 kPa	YES	25→90→25
1.26 ± 0.05	K6-SW-I250	OC	6	250 kPa	1500 kPa	NO	25
1.23 ± 0.05	K6-SW-IT250	OC	6	250 kPa	1500 kPa	YES	25→90→25

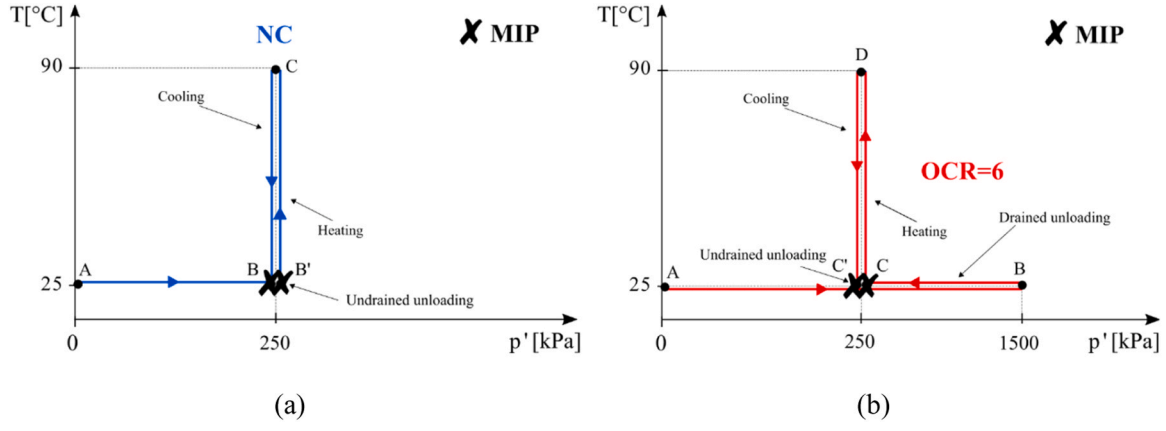

Fig. 3. Thermomechanical paths for (a) KI-SW-IT250 and (b) K6-SW-IT250.

Confining and back pressures are imposed by two GDS volume-pressure advanced controllers. A controller used to impose the cell pressure is also employed to measure the volume of confining liquid moving in and out of the cell, from which the volumetric deformation of the sample can be only qualitatively inferred given the thermal expansion of the equipment. The vertical and radial displacements are locally measured with Hall effect transducers glued on the neoprene membrane covering the sample. This measurement strategy was adopted to obtain

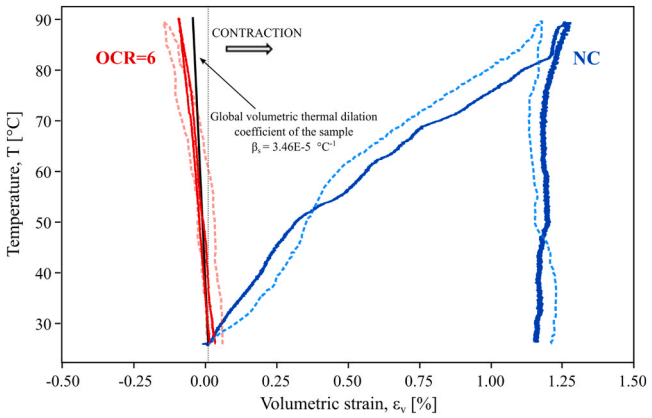

Fig. 4. Measured volumetric strain of Speswhite Kaolin clay upon a heating-cooling cycle for normally consolidated (K1-SW-IT250, blue curves) and over-consolidated samples (K6-SW-IT250, red curves).

reliable volumetric strain estimates under thermal loading, avoiding uncertainties associated with fluid-based volume measurements that are exacerbated by temperature variations (more details on the local transducers and their temperature compensation can be found in Appendix 1). Diaphragm pressure transducers measure pore water pressure on the sample's top and bottom.

The heating system comprises a temperature probe installed in the cell, which gives a feedback signal to control the power input supplied to the heaters and required to maintain a target cell's water temperature (overall precision ±0.1°C). The whole system is located in a temperature-controlled room maintained at a constant temperature of 20 ± 1°C. Temperature close to the specimen was measured through 8 K-type thermocouples distributed over the neoprene membrane (overall precision ±2.2°C).

Finally, an acquisition system continuously collected and stored the measured pressures, the temperature close to the sample, the water volume exchanged, and the vertical and radial displacements measured by the Hall effect transducers.

3.2. Experimental program

3.2.1. Macroscopic testing

Temperature-controlled isotropic compression tests were conducted following the four thermomechanical paths shown in Table 2 and Fig. 3. The initial void ratio, e_{ini}, reported in Table 2 corresponds to the void ratio of the clay cake (consolidated at 200 kPa in the consolidometer) from which each specimen was extruded prior to installation in the isotropic compression cell. The uncertainty associated with e_{ini} arises from (i) the determination of the water content used to compute the void ratio, and (ii) the fact that each thermomechanical path was repeated on two specimens prepared from two different clay cakes. The reported values therefore represent the average of the two measurements and should be interpreted within an uncertainty band reflecting these sources of variability.

Ambient-temperature isotropic compression was conducted along two distinct stress paths (K1-SW-I250 and K6-SW-I250 in Table 2). In the first case, the specimen was loaded to mean effective stress, p'= 250 kPa (K1-SW-I250, A-B in Fig. 3a). In the second case, the specimen was loaded to 1500 kPa and then unloaded to 250 kPa, reaching an OCR equal to 6 (K6-SW-I250, A-B-C in Fig. 3b).

Two additional thermomechanical paths involved identical stress history followed by a drained thermal cycle (25°C → 90°C → 25°C at a constant heating/cooling rate of 3°C/h) applied at a constant mean effective stress of 250 kPa (K1-SW-IT250, B-C-B′ in Fig. 3a and K6-SW-IT250, C-D-C′ in Fig. 3b). In these cases, the specimens were either fully consolidated (OCR = 1) or allowed to swell (OCR = 6) prior to heating. A constant heating at 3°C/h ensures a homogeneous temperature field and no significant pore water pressure build up (drained conditions) in the sample. Further details on the heating rate choice can be found in the thermal calibration in Appendix 1.

After thermo-mechanical or purely mechanical loading, all the samples were rapidly unloaded under undrained conditions to preserve as much as possible the sample microstructure. All macroscopic tests were performed twice to ensure the repeatability of the results.

3.2.2. Microstructural investigation

The post-mortem microstructure of the samples before and after the heating-cooling cycle (marked with a cross in Fig. 3a and Fig. 3b) was analysed using MIP and SEM to gain insight into the micro-mechanisms underlying the reversible and non-reversible thermomechanical behaviour of the clay.

Mercury intrusion porosimetry tests and scanning electron microscope observations were performed on dehydrated samples. After undrained unloading, the samples were divided into small specimens of approximately 1.5 cm^3. The small specimens were individually dehydrated using the freeze-drying technique, which involved rapid freezing in cryogenic liquid (liquid nitrogen, freezing temperature: −210 °C) and subsequent sublimation in a controlled vacuum chamber (Alpha 2–4 LDplus lyophilisation apparatus).

Freeze-drying is widely considered the most effective dehydration technique for preserving clay microstructure prior to MIP and SEM analysis. By removing pore water through sublimation, it minimizes capillary stresses and prevents fabric collapse that typically occurs during air- or oven-drying[29-31]. However, as demonstrated by Di Remigio et al. (2021)[32], no dehydration method is entirely free from artefacts. The extent of microstructural disturbance depends strongly on the clay's stress history, with soft, normally consolidated clays proving more vulnerable than heavily overconsolidated ones. Despite these inherent limitations, their comparative study confirmed that freeze-drying produces the least alteration of pore structure relative to other drying methods, thereby supporting its adoption in the present work.

MIP tests were carried out using a Poremaster-60 manufactured by Quantachrome Instruments. The equipment is designed to measure pore entrance size from about 1000 μm to 0.003 μm corresponding to 1.5–420,000 kPa mercury intrusion pressure respectively.

SEM images were obtained using a LEO Ultra 55 SEM at the Chalmers Materials Analysis Laboratory (CMAL). After freeze drying, additional fractures were generated to reveal the internal surfaces parallel to the consolidation direction of the clay deposit (vertical), unaffected by the wire cutting of the test specimen. The topography of the samples was quantified by scanning the gold-coated opened fractures with a focused electron (15 kV). The measurements were acquired in high vacuum mode to achieve the highest resolution.

4. Results and discussion

4.1. Thermomechanical volumetric response

The volumetric response of Speswhite Kaolin clay upon heating and cooling is shown in Fig. 4 for the normally consolidated specimen (blue path in Fig. 3a, K1-SW-IT250 9 in Table 2) and the overconsolidated specimen (red path in Fig. 3b, K6-SW-IT250 in Table 2). The non-isothermal phase were carried out at the same mean effective stress but under different loading histories of the material to investigate the effect of the OCR.

The volumetric strain was computed from the local axial and radial displacement measured ($\varepsilon_v = 2\varepsilon_r + \varepsilon_a$). The displacement measurements were corrected according to the thermal calibration of the sensors reported in Appendix 1. Two tests on two different samples belonging to two different clay cakes were conducted for each thermomechanical path to assess the repeatability of the results. For each

Table 3
Summary of the average final void ratio at the end of the test for all the thermomechanical paths tested.

Test ID	Stress history	OCR	Confinement stress, p'_c	Preconsolidation stress, p'_p	Thermal cycle, TC	Final void ratio, e_{fin}
K1-SW-I250	NC	1	250 kPa	250 kPa	NO	1.20 ± 0.05
K1-SW-IT250	NC	1	250 kPa	250 kPa	YES	1.14 ± 0.05
K6-SW-I250	OC	6	250 kPa	1500 kPa	NO	0.93 ± 0.05
K6-SW-IT250	OC	6	250 kPa	1500 kPa	YES	0.91 ± 0.05

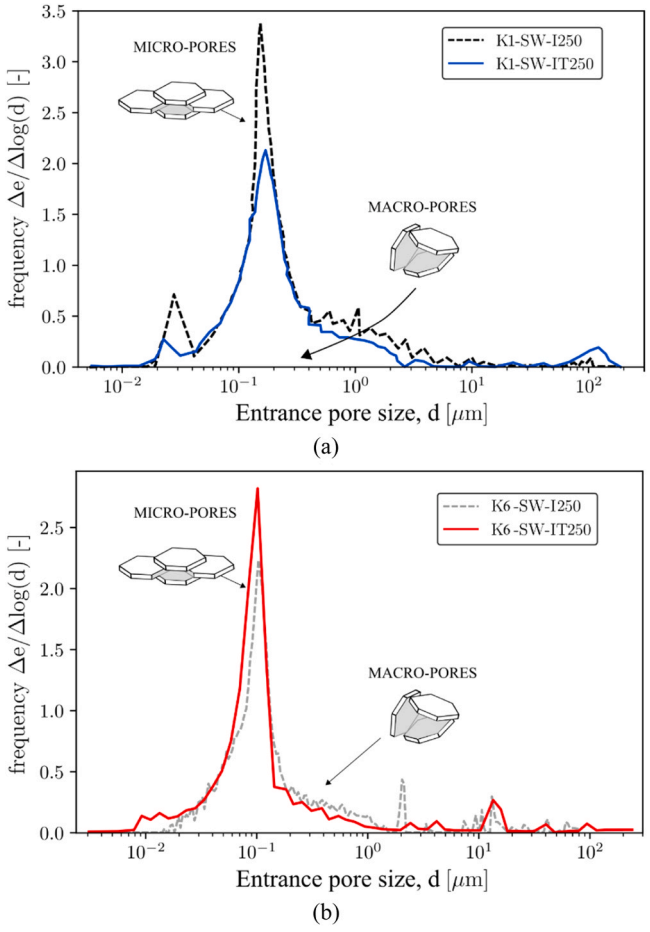

Fig. 5. Pore size evolution after one heating-cooling cycle performed in (a) NC and (b) OC conditions. The PSDs obtained post-mortem from thermomechanically loaded samples (after heating, solid lines) are compared to the ones of solely mechanically loaded samples (before heating, dashed lines).

thermomechanical path, the final void ratio after the complete heating–cooling cycle, computed separately from the two responses reported in blue and red in Fig. 4, is reported in Table 3.

Local strain measurements reveal an anisotropic response during thermal loading, with axial contraction exceeding radial contraction during heating. This discrepancy depends on the stress history, being more pronounced at stress levels close to the vertical stress at which the reconstituted samples were prepared (200 kPa), and progressively diminishing at higher isotropic stress. This trend reflects the gradual reduction of fabric-induced cross-anisotropy with increasing pre-loading also shown by Hueckel and Pellegrini[33]. Further details on strain anisotropy during thermal loading of normally consolidated kaolin can be found in Casarella et al.[34].

Thermal contraction is observed in normally consolidated conditions. During heating, the NC sample reduces its volume non-linearly with temperature. During cooling, the soil does not recover the deformation accumulated upon heating. The apparent slight expansion upon temperature decreases in Fig. 4 falls in the range of spurious variation of

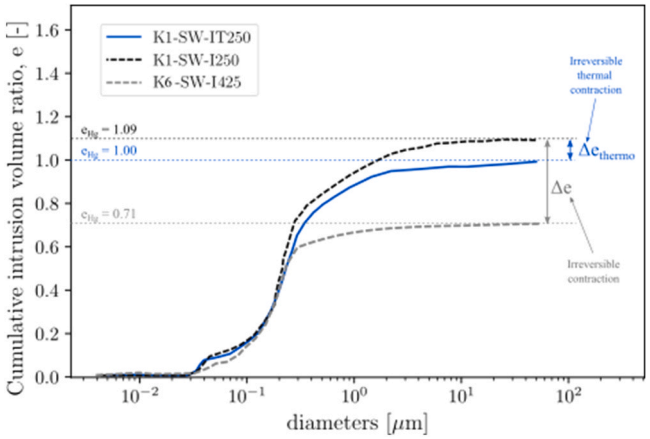

Fig. 6. Comparison of the cumulative PSDs of NC clay subjected to thermomechanical loading (K1-SW-IT250, blue line) and heavy isotropic compression (K6-SW-I250, dashed grey line).

volumetric strain associated with the error of temperature correction as reported in Appendix 1, not allowing any conclusive observations on the expansive or contractive behaviour of the material upon cooling. While partial re-adsorption of physically bound water on kaolinite particle surfaces may, in principle, contribute to a minor reversible expansion, the associated deformation cannot be reliably distinguished from measurement uncertainty. The behaviour over the whole cycle indicates the irreversibility of strain due to thermal loading, which is referred to as thermal hardening[3].

In contrast to the NC state, heating produces mainly reversible dilation in the highly overconsolidated (OC) sample. The results presented in Fig. 4 are consistent with the experimental data in the literature [7,8,3,35,9].

While the present study focuses on isotropic thermomechanical loading, for constitutive modelling purposes, complementary mechanical characterisation of Speswhite Kaolin clay under triaxial loading conditions is available in Zhuang et al.[36] and Robinson et al.[37].

4.2. Microstructure evolution upon heating

The Pore-Size Distribution (PSD) obtained through the MIP tests is shown in Fig. 5 (MIP tests after heating-cooling cycle were carried out on the samples represented by continuous curves in Fig. 4). Two different classes of pores may be identified, micro-pores distributed around the modal value of ~ 0.1 μm and macro-pores associated with the tail of the PSD on the right side of the modal value of the order of 1 μm[26].

The modal size reflects the pore generated by the staggered face-to-face particle arrangement schematically illustrated in Fig. 5, as the modal value of ~0.1 μm is of the same order of magnitude as the particle thickness (shown later in Fig. 7). The pore sizes forming the tail of the PSD are instead associated with edge-to-face arrangements, since their characteristic size is comparable to the particle width (also shown in Fig. 7)

An additional secondary peak observed at smaller entrance pore sizes (~ 20 nm) falls within the micro-porosity range and likely reflects a finer sub-population of inter-particle pores associated with face-to-face

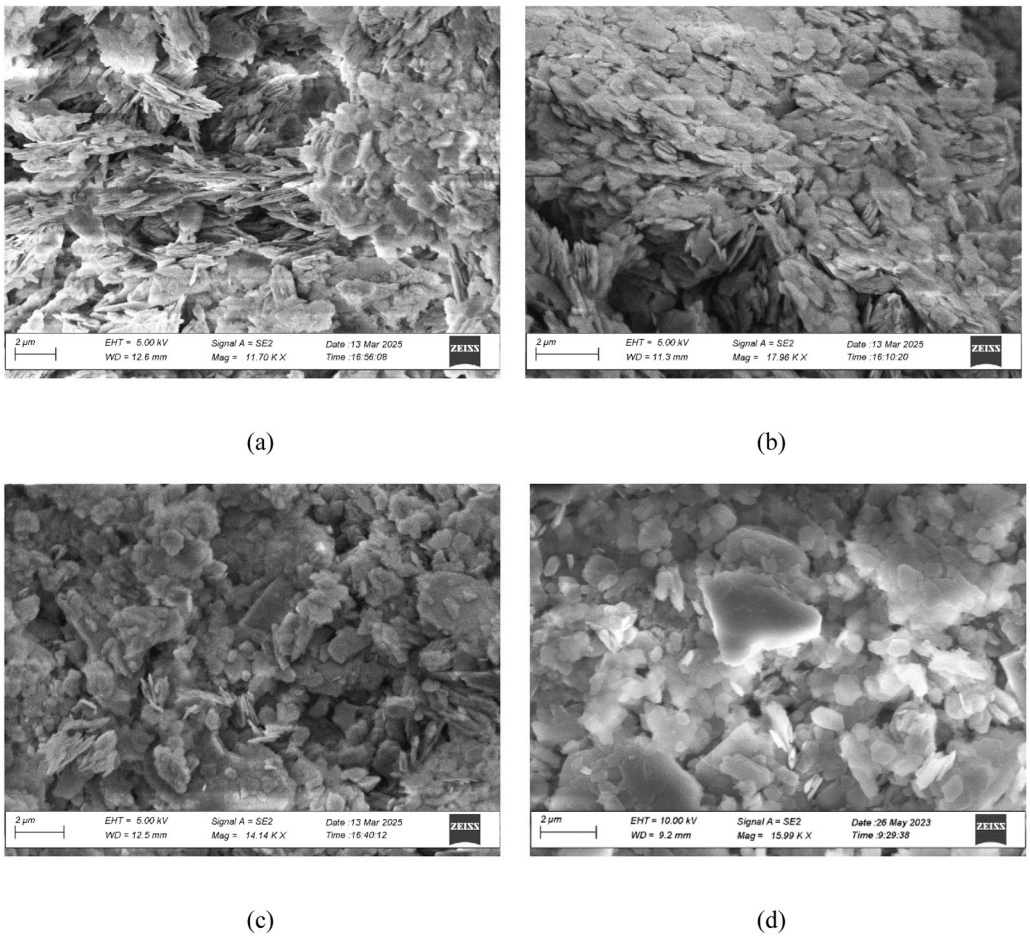

Fig. 7. SEM observations of (a) K1-SW-I250, (b) K1-SW-IT250, (c) K6-SW-I250 and (d) K6-SW-IT250.

configurations; however, due to the logarithmic spacing of MIP data and the limited reliability of mercury intrusion at small pore sizes, no quantitative distinction between micro-pore sub-populations is attempted.

In Fig. 5a, it can be observed that the pore size distribution of the sample normally consolidated to 250 kPa and then subjected to a

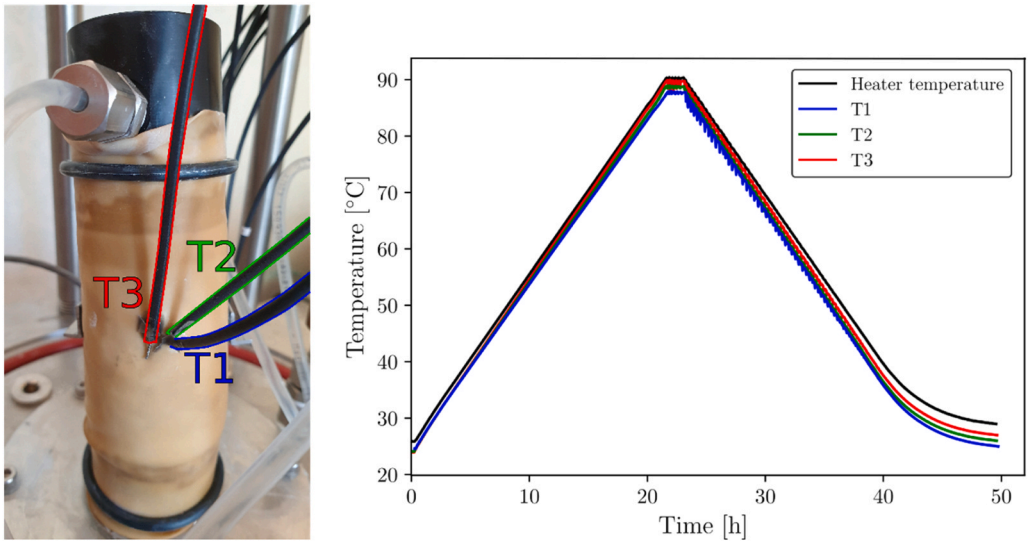

Fig. 8. (a) Location of the thermocouples for the thermal calibration process; (b) Differences in temperature recorded between the heating system, the centre of the sample (T1) and the external sample perimeter inside and outside of the neoprene membrane (T2 and T3, respectively).

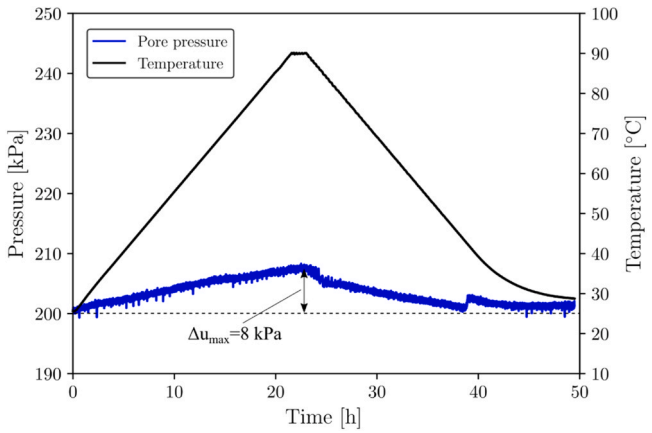

Fig. 9. Excess pore water pressure fluctuations measured on the top of the sample upon a thermal loading cycle of $\Delta T = \pm 65$ °C at a constant heating/cooling rate of 3 °C/h.

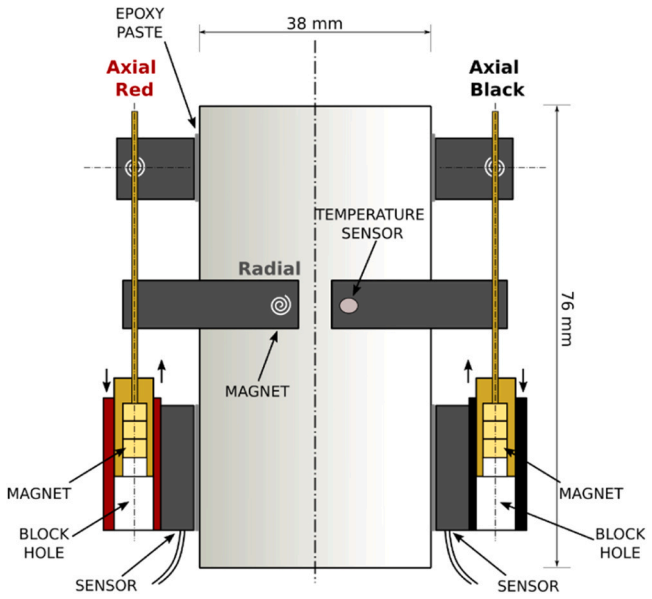

Fig. 10. Sketch of the disposition of the Hall effect transducers on a vertical section of the sample.

heating-cooling cycle (K1-SW-IT250) has the same micro-pore distribution as the sample normally consolidated to 250 kPa (K1-SW-I250). The apparent variations in the amplitude of the micropore peak between thermally loaded and unloaded samples should be interpreted with caution: because the PSD is discretised on a logarithmic pore-size scale, the sharpness of the micropore peak and the intrinsic limitations of mercury intrusion at small pore sizes preclude a reliable quantitative comparison of micropore frequency. On the other hand, the distribution of the macro-pores shifts to the left, indicating a reduction of the macropore sizes following thermal plastic deformation.

In contrast, the two samples in Fig. 5b show similar PSDs (K6-SW-I250 and K6-SW-IT250). No significant changes in either macro-pores or micro-pores are observed. The post-mortem observations reveal that, if any microstructure change occurs when the temperature is increased, this is entirely reversible.

Fig. 6 shows the cumulative pore-size distribution associated with the normally consolidated sample (K1-SW-I250, dashed black curve), the normally consolidated sample following thermal plastic deformation (K1-SW-IT250, continuous line), and the overconsolidated sample (K6-SW-I250, dashed gey curve). The PSD up to 200 nm remains essentially the same for the three specimens and variations only occur in the macroporosity range (>200 nm).

Mechanical yielding (irreversible mechanical contraction) is associated with a reduction of the macro-pores (from K1-SW-I250 to K6-SW-I250). Thermal yielding (irreversible thermal contraction) is also associated with a reduction of the macro-pores (from K1-SW-I250 to K1-SW-IT250). Despite the difference in magnitude, an akin microstructural process appears to control the plastic deformation of the clay, regardless of whether this is induced mechanically or thermally.

SEM imaging was utilised to qualitatively verify changes in particle arrangement. Fig. 7 compares SEM images of the four tested samples. The normally consolidated sample that did not experience thermal loading (K1-SW-I250, Fig. 7a) exhibits an open 'flocculated' particle configuration with visible edge-to-face contacts between particles or clusters of staggered particles. The fabric of the thermally treated normally consolidated sample (K1-SW-IT250, Fig. 7b) shows a reduction of particles/clusters in edge-to-face contact and a reduction of macropores. This is consistent with the MIP results in Fig. 6.

On the other hand, both the overconsolidated samples (Fig. 7c and Fig. 7d) show particles and clusters mostly in face-to-face configuration, as opposed to the normally consolidated samples in Figs. 7a and 7b. No significant changes are evident when comparing the fabric of the thermo-mechanically loaded sample (K6-SW-IT250, Fig. 7d) with the fabric of one that has not experienced any thermal load (K6-SW-I250, Fig. 7c).

SEM images thus support qualitatively the microstructural interpretation drawn quantitatively from MIP and macroscopic strain measurements. These findings are consistent with the observations of Hattab et al. (2011)[22], which show that isotropic compression of samples initially formed under one-dimensional loading not only drives the evolution of fabric from anisotropic to isotropic but also promotes increased face-to-face aggregation.

4.3. Discussion

Pedrotti and Tarantino (2018)[26] have proposed that micro-pores distributed around the modal value of the PSD are associated with particles in non-contact configuration, that is, those interacting only by the overlap of the repulsive electrical field generated by the negatively charged faces. Particles in non-contact configuration undergo elastic deformation, i.e., they approach each other during mechanical loading and rebound upon mechanical unloading. On the other hand, macro-pores are associated with contact configuration caused by the attraction between the positively charged edge and the negatively charged face of the clay particles. Plastic mechanical deformation was observed to correspond to the loss of macro-pores and, hence, was associated with slippage at the edge-to-face contact.

The pore-size distribution of the over consolidated (OC) specimen before heating as shown in Fig. 5b is characterised by the dominance of micro-pores and a relatively small fraction of macro-pore (tail of the PSD). The high pre-consolidation stress has caused most of the particles to arrange in face-to-face configuration. Under these conditions, heating is expected to induce purely elastic changes in the separation distance between particles in face-to-face configuration. This interpretation aligns with the numerical analysis of Di Donna et al.[24], who showed using 3D DLVO interactions that increasing temperature in face-to-face arrangements produces a reversible increase in separation distance (elastic rebound) governed by temperature-dependent electrostatic repulsion. The experimental evidence supports this: the OC specimen exhibits macroscopic reversible thermal dilation upon heating (Fig. 4), and its PSD remains essentially unchanged after the thermal cycle (Fig. 5b), confirming the absence of plastic rearrangement.

On the other hand, the PSD of the normally consolidated (NC) sample before heating in Fig. 5a shows a substantial fraction of macropores associated with a predominance of edge-to-face contacts, which are mechanically weaker and susceptible to slippage. Thermal loading in NC

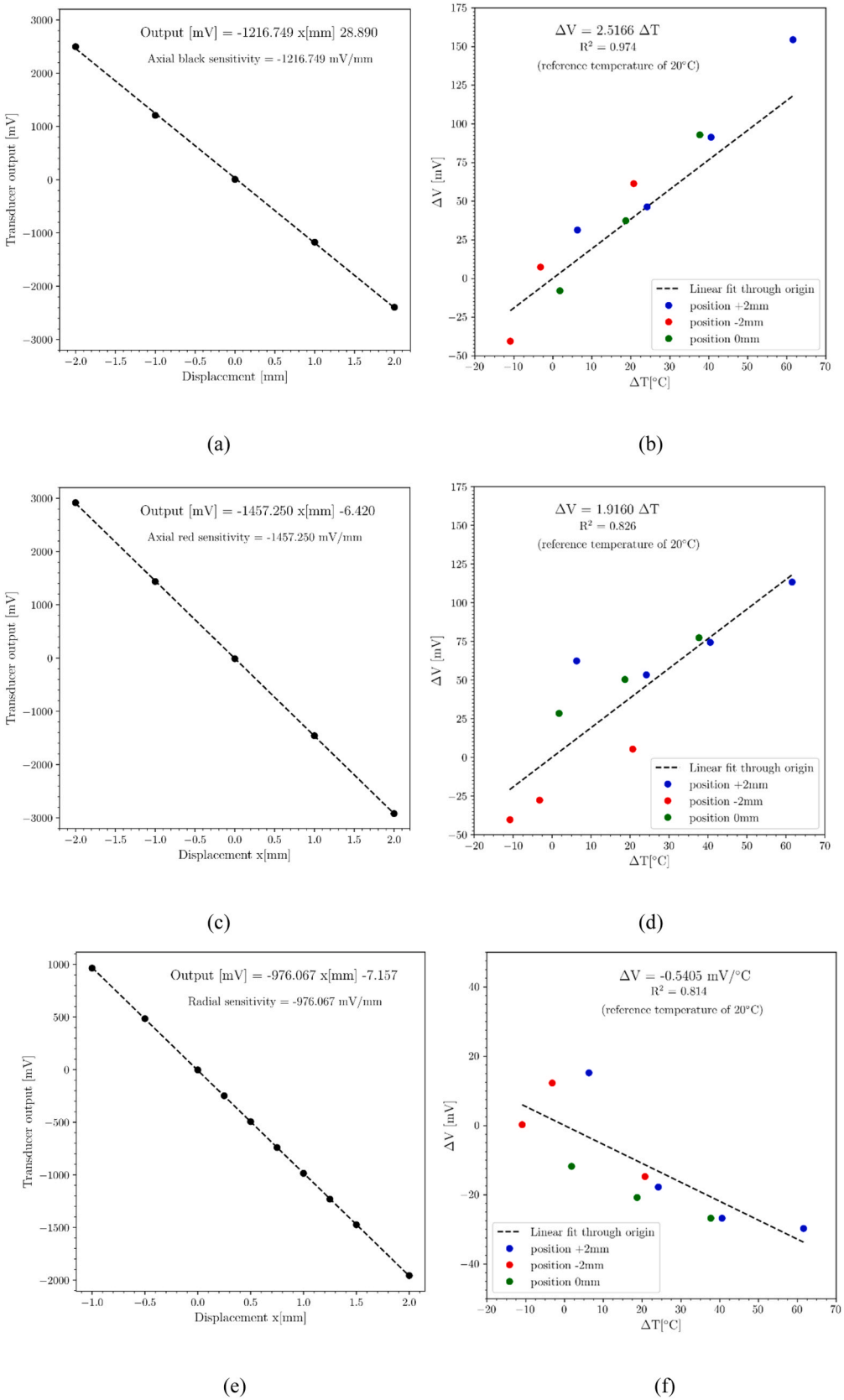

Fig. 11. Calibration of the (a) axial black, (c) axial red and (e) radial Hall effect local transducers against a reference LVDT transducer. Thermal calibration of the (b) axial black, (d) axial red and (f) radial Hall effect local transducers in three different positions: 0 mm, + 2 mm and −2 mm.

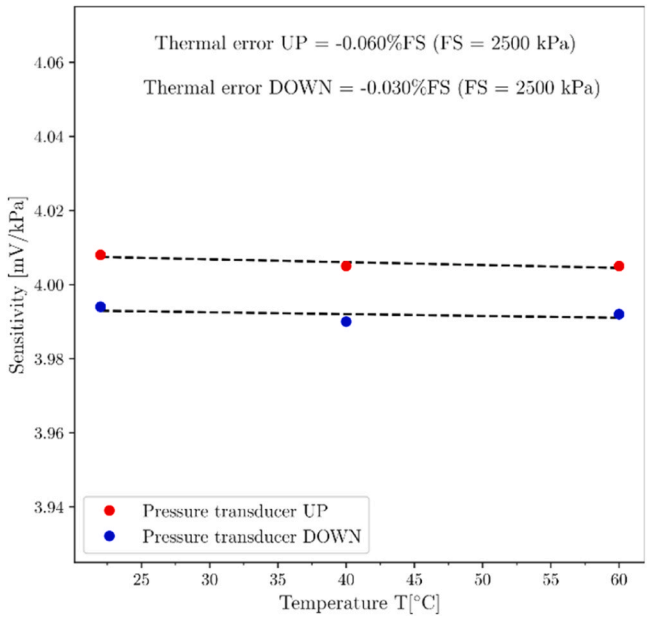

Fig. 12. Temperature effect on the sensitivity of pressure transducer UP and DOWN.

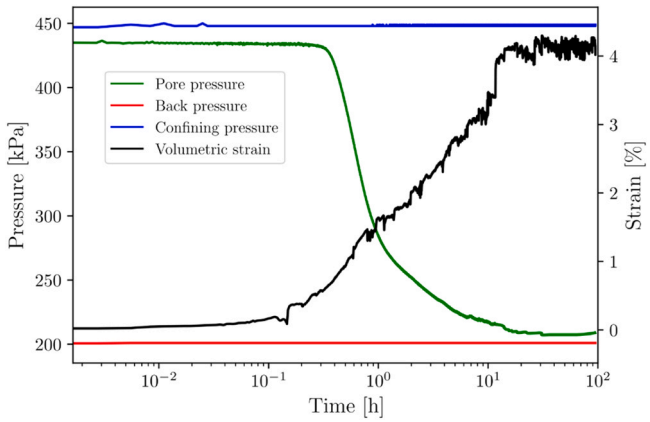

Fig. 13. Dissipation of excess of pore pressure over an isotropic loading step of 250 kPa.

conditions induces a clear irreversible volumetric contraction (Fig. 4), consistent with a thermally-induced reduction in resistance to particle slippage. This mechanism is also predicted by Di Donna et al.[24], who demonstrated numerically (using 3D DLVO interactions) that an increase in temperature reduces the shear resistance of edge-to-face contact interactions, promoting irreversible rearrangements. The MIP results provide quantitative confirmation: after the heating–cooling cycle, the NC sample shows a distinct shift of the macropore tail toward smaller pore sizes (Fig. 5a). Importantly, the micropore region remains essentially unchanged, indicating that thermal plasticity is governed by the collapse of macropores rather than compression of the clay platelets themselves.

A comparison between the final void ratios obtained from macroscopic measurements (Table 3) and those inferred from cumulative pore-size distributions (Fig. 6) shows that MIP consistently underestimates the absolute void ratio of the material. This outcome is well established and reflects inherent limitations of mercury intrusion techniques, particularly their incomplete access to the smallest pores and poorly connected domains, which results in an underestimation of total porosity[38,39].

The effect is more pronounced in the thermally treated sample (K1-SW-IT250) and even more in the overconsolidated sample (K6-SW-I250), where the pore structure is dominated by smaller, tighter throats that hinder mercury intrusion. Consequently, void-ratio variations inferred from MIP tend to exaggerate the magnitude of both mechanical and thermal changes relative to macroscopic measurements. This discrepancy is further compounded by experimental uncertainty in the initial void ratio, since MIP analyses necessarily involve different specimens taken from separate clay cakes.

Despite these systematic differences, the trends captured by MIP remain consistent with macroscopic observations: both mechanical and thermal loading reduce macro-porosity, and the relative magnitude of this reduction reflects the macro-scale response.

5. Conclusions

This paper has presented the results of a multi-scale investigation aimed at exploring the micro-mechanism leading to the different response of observed in the literature for normally consolidated (NC) and over-consolidated (OC) clay subjected to thermal loading, i.e., elastic expansion for OC clay and plastic compression for NC clay. To this end, temperature-controlled isotropic compression tests on Speswhite Kaolin clay were coupled with Mercury Intrusion Porosimetry (MIP) measurements and Scanning Electron Microscope (SEM) observations.

In line with previous findings in the literature, the clay exhibited irreversible contraction under NC conditions and reversible expansion under highly OC conditions. The pore size distribution data highlighted that the thermoplastic response of NC clay appears to be associated with a decrease in volume of clay macropores, indicating loss or rearrangement of edge-to-face particle contacts. Although MIP systematically underestimates absolute void ratio due to incomplete mercury accessibility, the observed direction and relative magnitude of microstructural changes remain consistent with macroscopic strains. In OC conditions, the pore size distributions before and after heating were essentially unchanged, corroborating that thermal deformation is elastic and confined to reversible adjustments in the separation distance of particles in face-to-face configuration.

The microstructural evidence confirms the emerging view also predicted numerically by Di Donna et al.[24] that the same particle-scale mechanisms governing mechanical yielding and elastic rebound are mobilised under thermal loading. Specifically, thermal plasticity in NC clay stems from temperature-induced weakening of edge-to-face slippage resistance, while thermal elasticity in OC clay reflects reversible changes in DLVO-governed inter-particle forces in face-to-face arrangements. This study therefore provides experimental validation for the hypothesis that thermal volumetric deformation under constant stress activates the same microscale processes that drive mechanically induced volumetric deformation.

From a modelling perspective, the main contribution of this study is to provide a physically consistent interpretation of the macroscopic thermomechanical volumetric behaviour of clay. The high level of experimental control makes the experimental dataset presented particularly suitable for validation of particle-scale models. In particular, the uniform particle size distribution, controlled pore fluid environment, and reproducible fabric generated by sedimentation and vertical consolidation enable direct comparison with simulations based on the Discrete Element Method (DEM) or Coarse-Grained Molecular Dynamics (CGMD). In this regard, recent developments in experimental clay micromechanics, such as those presented in Casarella et al.[40], open promising perspectives for extending the present findings. When applied to thermomechanical loading, such approaches could directly resolve and quantify the evolution of particle contact networks that are inferred in this study. The present work therefore establishes a necessary experimental and conceptual framework upon which these advanced 3D observations can build, ultimately contributing to closing the

long-standing gap between particle-scale mechanisms and their representation within continuum constitutive models for thermomechanical behaviour of clay.

CRediT authorship contribution statement

Alessandro Tarantino: Writing – review & editing, Supervision, Conceptualization. **Angela Casarella:** Writing – original draft, Methodology, Investigation, Formal analysis, Data curation, Conceptualization. **Alice di Donna:** Writing – review & editing, Supervision, Project administration, Funding acquisition, Conceptualization.

Declaration of Competing Interest

The authors declare the following financial interests/personal relationships which may be considered as potential competing interests: Alice Di Donna reports financial support was provided by Agence nationale de la recherche. If there are other authors, they declare that they have no known competing financial interests or personal relationships that could have appeared to influence the work reported in this paper.

Acknowledgements

This work was funded by the ANR project GEO2 (ANR-19-CE05–0003–01). The Laboratory 3SR is part of the LabEx Tec 21 (Investissement d'avenir – grant agreement n. ANR-11-LABX-0030).

APPENDIX 1. – Temperature Calibration of the test equipment

A.1 Temperature uniformity and excess pore-water pressure dissipation conditions

Preliminary calibration tests were performed to ensure the uniformity of the temperature field inside the sample. The calibration procedure consisted in imposing a temperature rate on the heating system and monitoring the difference in temperature recorded between three thermocouples (Fig. 8a) inserted in the centre of the sample (T1) and close to its lateral surface on the inside and the outside of the neoprene membrane (T2 and T3 respectively). For the calibration procedure only, the thermocouples T1 and T2 were let to pass through tiny holes in the neoprene membrane. To isolate the cell water from the pore-water, the holes in the membrane were carefully sealed with waterproof sealant. Starting from a constant temperature of 25ºC, a thermal loading of $\Delta T = \pm 65$ºC was imposed by the electric heater at a rate of 3 ºC/h. The thermal loading rate was chosen accordingly to the hydraulic conductivity calculated for a Spweswhite Kaolin clay sample isotropically loaded up to 1500 kPa (the highest isotropic stress applied in the experimental campaign presented in this chapter), being equal to $0.6 \cdot 10^{-9}$ m/s (refer also to Al-Tabbaa and Wood[41] for comparison).

Fig. 8b shows the evolution of T1, T2 and T3 compared to the temperature measured on the surface of the heating system. At the selected heating rate, the increase in temperature inside the sample closely follows the temperature imposed on the heater. Almost no time lag is required to reach a steady-state temperature inside the specimen. Moreover, negligible differences in temperature monitored by the sensor placed in the middle of the sample (T1) and the one located on the external perimeter (T2) are recorded (the maximum recorded difference between T1 and T2 is 2.0ºC, which is lower than the K-type thermocouples maximum error). ensures the uniformity of the temperature field when heating at the constant rate of 3 ºC/h was therefore considered satisfactory.

The same thermal loading/unloading was performed on a sample subjected to a constant isotropic stress of 1500 kPa to measure the excess pore water pressure Δu [kPa]. The test to measure the build-up of the excess pore-water pressure was performed on the clay sample isotopically compressed to 1500 kPa, as this sample has the lowest consolidation coefficient among the ones tested in this experimental campaign. The pore water pressure was measured at the top of the sample where no drainage was allowed and at the bottom of the sample where water pressure was maintained constant using the GDS controller. Fig. 9 shows minor fluctuations of the excess of pore pressure Δu (measured on top of the sample) around 0 kPa. Therefore, a heating/cooling rate of 3 ºC/h also satisfies the drained conditions. This thermal loading rate is therefore selected for all the thermomechanical paths followed in the experimental campaign presented in Section 3.2.

A.2 Temperature compensation of the sensors

A.2.1 Hall effect transducers

One radial and two axial Hall effect transducers were employed in this study to measure displacements locally. The Hall effect sensor detects the magnetic flux variations occurring due to the displacement of a magnet mounted at the opposite end of the transducer. The nominal calibrated working range of the transducers is ±2 mm, with an accuracy of ±0.25% of the scale range. Sensors were directly glued onto the neoprene membrane according to the schematic layout shown in Fig. 10. Two-component epoxy paste adhesive, Araldite 2014–2 (nominal working temperature range between −40 ºC and +140 ºC) was employed for bonding the sensors.

All the pieces of the equipment are calibrated at 20ºC against a reference LVDT transducer (Keysight 34460 A multimeter). The calibration curves axial black, axial red and radial are shown in Fig. 11a, Fig. 11c and Fig. 11e, respectively.

Since all the displacement transducers are exposed to high temperatures, they need to be temperature-compensated in the range 20ºC to 90ºC. A temperature sensor (operating range: 0 −200 ºC, overall precision ±0.1ºC) was installed on the radial jaw (see Fig. 10) to detect the radial sensor temperature. Firstly, the temperature sensor located on the radial jaw was calibrated by placing the radial transducer in a climatic chamber and varying the internal temperature from 0 ºC to 120 ºC. Then, the calibration procedure consisted in fixing the magnetic rod of each transducer at a given position inside the block hole (-2mm, 0 mm, +2 mm), set a temperature in the climatic chamber and let it stabilise until the temperature sensor on the radial jaw reached thermal equilibrium. At this point, the acquisition system recorded the local transducer signal output. Different temperatures were set following the same procedure. The difference in voltage (upon a thermal cycle from 10 ºC to 80 ºC, reference temperature 20 ºC) between the value just acquired and the one registered when having the transducer in the same position at 20 ºC is shown in Fig. 11b, Fig. 11d and Fig. 11f for axial black, axial red and radial, respectively. Based on the temperature-calibration data in Fig. 11, it was assumed that temperature affects the offset (intercept) but not the sensitivity (slope) of the calibration curve. The linear fittings in Fig. 11b, Fig. 11d and Fig. 11f were used to correct the offset of the linear

calibration permed at 20°C in Fig. 11a, Fig. 11c and Fig. 11e.

By examining the spread of the residuals (i.e., the differences between observed and fitted values) in Fig. 11b, Fig. 11d and Fig. 11f, one can calculate the standard deviation of the error in the estimation of the volumetric strain associated with the error of temperature correction, denoted as $SD_{\Delta\varepsilon_v}$.

$$SD_{\Delta\varepsilon_v} = \sqrt{\left(\frac{\left(SD_{\delta_{a,\ Red}} + SD_{\delta_{a,\ Black}}\right)}{H_0}\right)^2 + \left(\frac{SD_{\delta_r}}{D_0}\right)^2} \approx 0.035\% \quad (1)$$

where H_0 [mm] and D_0 [mm] are the reference height and diameter of the sample, respectively. $SD_{\delta_{a,Red}}$ [mm], $SD_{\delta_{a,Black}}$ [mm] are the standard deviations of the error in the estimation of the axial displacement using the axial red and the axial black transducer, respectively, while SD_{δ_r} [mm] represents the standard deviation of the error in radial displacement measured by the radial transducer.

A.2.1 Diaphragm type pressure transducers

Two diaphragm type pressure transducers (named UP and DOWN), with an operating range up to 2.5 MPa, are used to measure pore water pressure on the top and on the bottom of the sample. The voltages recorded on the pressure transducers need to be temperature-compensated. To do so, the diaphragm type pressure transducers, in contact with circulating water at 40 °C and 60 °C, are verified by comparison technique with another certified pressure transducer (MCX II - Druck portable documenting calibrator, guaranteed to an accuracy of ±0.05% of the scale range 0–2.5 MPa).

Fig. 12 shows the temperature effect on the sensitivity for both the transducer. The calculated deviations due to temperature are considerably small (-0.060%FS and −0.030%FS, FS = 2500 kPa) and they are therefore neglected in all the experiments described in Section 3.2.

APPENDIX 2. – Isotropic compression

After full saturation of the samples (verified using the B-value test), drained conditions were re-established by opening the bottom drainage valve. Due to the high permeability of kaolin clay, drainage was permitted only from the bottom while pore pressure at the top was continuously monitored using a diaphragm transducer.

The specimens were then subjected to isotropic loading, or to isotropic loading followed by unloading, until the desired confining pressure and overconsolidation ratio were achieved. A constant back pressure of 200 kPa was maintained throughout loading and unloading stages.

For target mean effective stresses exceeding 250 kPa, confining pressure was increased in increments of 250 kPa. At each increment, sufficient time was allowed for dissipation of excess pore water pressure (see Fig. 13). The consolidation period for each 250 kPa loading step was approximately 120 h. Unloading was also performed in 250 kPa steps.

Data availability

Data will be made available on request.

References

1. Towhata I, Kuntiwattanaku P, Seko I, Ohishi K. Volume change of clays induced by heating as observed in consolidation tests. *Soils Found*. 1993;33(4):170–183. https://doi.org/10.3208/sandf1972.33.4_170.
2. Sojoudi M, Li B, Norouzi E. Finite element modeling of thermo-hydro-mechanical coupled processes in clay soils considering bound water dehydration. *Acta Geotech*. 2024;19:3769–3784. https://doi.org/10.1007/s11440-024-02262-7.
3. Hueckel T, Baldi G. Thermoplasticity of saturated clays: experimental constitutive study. *J Geotech Geoenviron Eng ASCE*. 1990;116(12):1778–1796. https://doi.org/10.1061/(ASCE)0733-9410(1990)116:12(1778).
4. Murphy KD, Mccartney JS. Seasonal response of energy foundations during building operation. *S Geotech Geol Eng*. 2014;33. https://doi.org/10.1007/s10706-014-9802-3.
5. Laloui L, Di Donna A. Energy geostructures. *Innov Undergr Eng*. 2013. https://doi.org/10.1016/B978-0-08-100311-4.00007-8.
6. Sulem J, Lazar P, Vardoulakis I. Thermo-poro-mechanical properties of clayey gouge and application to rapid fault shearing. *Int J Numer Anal Methods Geomech*. 2007;31(3):523–540. https://doi.org/10.1002/nag.584.
7. Cekerevac C, Laloui L. Experimental study of thermal effects on the mechanical behaviour of a clay. *Int J Numer Anal Methods Geomech*. 2004;28:209–228. https://doi.org/10.1002/nag.332.
8. Abuel-Naga H, Bergado D, Bouazza A. Thermally induced volume change and excess pore water pressure of soft Bangkok clay. *Eng Geol*. 2007;89:144–154. https://doi.org/10.1016/j.enggeo.2006.10.002.
9. Campanella RG, Mitchell JK. Influence of temperature variations on soil behaviour. *Journal of the Soil Mechanics and Foundations Division*. 1968;94:609–734.
10. Di Donna A, Laloui L. Response of soil subjected to thermal cyclic loading: experimental and constitutive study. *Engineering Geology*. 2015;190:65–76. https://doi.org/10.1016/j.enggeo.2015.03.003.
11. Cui YJ, Sultan N, Delage P. A thermomechanical model for saturated clays. *Can Geotech J*. 2000;620:607–620. https://doi.org/10.1139/t99-111.
12. Graham J, Tanaka N, Crilly T, Alfaro M. Modified cam-clay modelling of temperature effects in clays. *Can Geotech J*. 2001;38(3):608–621. https://doi.org/10.1139/t00-125.
13. Hueckel T, Pellegrini R. Thermoplastic modeling of undrained failure of saturated clay due to heating. *Soils Found*. 1991;31(3):1765–1777. https://doi.org/10.3208/sandf1972.31.3_1.
14. Modaressi H, Laloui L. A cyclic thermoviscoplastic constitutive model for clays. *Proc Numer Models Geomech - NUMOG IV*. 1992;1:125–137. https://doi.org/10.1080/12795119.2001.9692328.
15. Baldi G, Hueckel T, Pellegrini R. Thermal volume changes of mineral-water system in low-porosity clay soil. *Can Geotech J*. 1988;25:807–825. https://doi.org/10.1139/t88-089.
16. Laloui L, François B. ACMEG-TS: a constitutive model for unsaturated soils under non-isothermal conditions. *Int J Numer Anal Methods Geomech*. 2008;32:933–944. https://doi.org/10.1002/nag.712.
17. Olson RE, Mesri G. Mechanisms controlling compressibility of clays. *J Soil Mech Found Div*. 1970;96(6):1863–1878. https://doi.org/10.1061/JSFEAQ.0001629.
18. Morin R, J. Silva A. The effects of high pressure-high temperature on some physical properties of ocean sediments. *J Geophys Res*. 1984;89:511–526. https://doi.org/10.1029/JB089iB01p00511.
19. Brochard L, Honório T, Vandamme M, Bornert M, Peigney M. Nanoscale origin of the thermo-mechanical behavior of clays. *Acta Geotech*. 2017;12:1261–1279. https://doi.org/10.1007/s11440-017-0596-3.
20. Revil A, Lu N. Unified water isotherms for clayey porous materials. *Water Resour Res*. 2013;49:5685–5699. https://doi.org/10.1002/wrcr.20426.
21. Guglielmi S, Cotecchia F, Cafaro F, Gens A. Microstructural changes underlying the macro-response of a stiff clay. In: Giovine P, Mariano P, Mortara G, eds. *Micro to MACRO Mathematical Modelling in Soil Mechanics. Trends in Mathematics*. Cham: Birkhäuser; 2018. https://doi.org/10.1007/978-3-319-99474-1_9.
22. Hattab M, Fleureau J-M. Experimental analysis of kaolinite particle orientation during triaxial path. *Int J Numer Anal Meth Geomech*. 2011;35:947–968. https://doi.org/10.1002/nag.936.
23. Houhou R, Sutman M, Sadek S, Laloui L. Microstructure observations in compacted clays subjected to thermal loading. *Eng Geol*. 2021;287, 105928. https://doi.org/10.1016/j.enggeo.2020.105928.
24. Di Donna A, Casarella A, Tarantino A. A micro-mechanical insight into the thermo-mechanical behaviour of clays. *Geomech Energy Environ*. 2024;38. https://doi.org/10.1016/j.gete.2024.100549.
25. Palomino AM, Santamarina JC. Fabric Map for Kaolinite: Effects of Ph and Ionic Concentration on Behavior. *Clays Clay Miner*. 2005:211–223. https://doi.org/10.1346/CCMN.2005.0530302.
26. Pedrotti M, Tarantino A. An experimental investigation into the micromechanics of non-active clays. *Géotechnique*. 2017;48(8):666–683. https://doi.org/10.1680/jgeot.16.P.245.

27. Burland JB. On the compressibility and shear strength of natural clays. *Geotechnique*. 1990;40(3):329–378. https://doi.org/10.1680/geot.1990.40.3.329.
28. Stallebrass SE, Atkinson JH, Mašín D. "Manufacture of samples of overconsolidated clay by laboratory sedimentation". *Geotechnique*. 2007;57(2):249–253. https://doi.org/10.1680/geot.2007.57.2.249.
29. Delage P, Pellerin FM. Influence de la lyophilisation sur la structure d'une argile sensible du Québec. *Clay Miner*. 1984;19(2):151–160. https://doi.org/10.1180/claymin.1984.019.2.03.
30. Romero Enrique, Simms Paul. Microstructure investigation in unsaturated soils: a review with special attention to contribution of mercury intrusion porosimetry and environmental scanning electron microscopy. *Geotech Geol Eng*. 2008;26:705–727. https://doi.org/10.1007/s10706-008-9204-5.
31. Penumadu D, Dean J. Compressibility effect in evaluating the pore-size distribution of kaolin clay using mercury intrusion porosimetry. *Can Geotech J*. 2000;37(2):393–405. https://doi.org/10.1139/t99-121.
32. Di Remigio G, Rocchi I Zania V. Scanning Electron Microscopy and Clay Geomaterials: From Sample Preparation to Fabric Orientation Quantification. *Applied Clay Science*. 2021;214:106249. https://doi.org/10.1016/j.clay.2021.106249.
33. Hueckel T, Pellegrini R. A note on thermomechanical anisotropy of clays. *Eng Geol*. 1996;41(1-4):171–180. https://doi.org/10.1016/0013-7952(95)00050-X.
34. Casarella A, Tarantino A, Di Donna A. *Effect of anisotropy on thermally-induced strains of kaolin clay*. In: *Proceedings of the 21st International Conference on Soil Mechanics and Geotechnical Engineering, Vienna*. 2026. 2026.
35. Di Donna A, Laloui L. Response of soil subjected to thermal cyclic loading: experimental and constitutive study. *Eng Geol*. 2015;190:65–76. https://doi.org/10.1016/j.enggeo.2015.03.003.
36. Zhuang PZ, Yu HS, Mooney SJ, Mo P. Loading and unloading of a thick-walled cylinder of critical-state soils: large strain analysis with applications. *Acta Geotech*. 2021;16:237–261. https://doi.org/10.1007/s11440-020-00994-w.
37. Robinson S, Brown MJ, Knappett J, Brennan A, Caballero DD, Arroyo M. The variation of large strain viscous rate effects from undrained triaxial element testing of Kaolin clay. *Acta Geotech*. 2025. https://doi.org/10.1007/s11440-025-02797-3.
38. Romero E, Villar MV, Lloret A. Thermo-hydro-mechanical behaviour of two heavily overconsolidated clays. *Eng Geol*. 2005;81(3):255–268. https://doi.org/10.1016/j.enggeo.2005.06.011.
39. Diamond S. Microstructure and pore structure of impact-compacted clays. *Clays Clay Miner*. 1971;19(4):239–249. https://doi.org/10.1346/CCMN.1971.0190405.
40. Casarella A, Pinzón G, Sadasivan V, et al. 3D particle aggregation in consolidated clay systems: insights from phase-contrast nano-holo-tomography. *Particuology*. 2026;112:271–283. https://doi.org/10.1016/j.partic.2026.02.002.
41. Al-Tabbaa A, Wood DM. Some measurements of the permeability of kaolin. *Géotechnique*. 1987;37(4):499–514. https://doi.org/10.1680/geot.1987.37.4.499.